Sensitivity of actuation dynamics on normal and lateral Casimir forces

Tajik, F.; Sedighi, M.; Palasantzas, G.

Published in:
Chaos

DOI:
10.1063/5.0065033

Sensitivity of actuation dynamics on normal and lateral Casimir forces: Interaction of phase change and topological insulator materials

Cite as: Chaos **31**, 103103 (2021); https://doi.org/10.1063/5.0065033
Submitted: 29 July 2021 • Accepted: 16 September 2021 • Published Online: 04 October 2021

F. Tajik, M. Sedighi and G. Palasantzas

Sensitivity of actuation dynamics on normal and lateral Casimir forces: Interaction of phase change and topological insulator materials

Cite as: Chaos **31**, 103103 (2021); doi: 10.1063/5.0065033
Submitted: 29 July 2021 · Accepted: 16 September 2021 ·
Published Online: 4 October 2021

F. Tajik,[1,2] M. Sedighi,[3] and G. Palasantzas[2,a)]

AFFILIATIONS

[1]Department of Physics, Faculty of Physics and Chemistry, Alzahra University, Tehran 1993891167, Iran
[2]Zernike Institute for Advanced Materials, University of Groningen, Nijenborgh 4, 9747 AG Groningen, The Netherlands
[3]Department of Mechanical Engineering, University of Sistan and Baluchestan, 98167-45845 Zahedan, Iran

[a)]**Author to whom correspondence should be addressed:** g.palasantzas@rug.nl

ABSTRACT

We investigated here the influence of the lateral and normal Casimir force on the actuation dynamics between sinusoidal corrugated surfaces undergoing both normal and lateral displacements. The calculations were performed for topological insulators and phase change materials that are of high interest for device applications. The results show that the lateral Casimir force becomes stronger by increasing the material conductivity and the corrugations toward similar sizes producing wider normal separation changes during lateral motion. In a conservative system, bifurcation and Poincaré portrait analysis shows that larger but similar in size corrugations and/or higher material conductivity favor stable motion along the lateral direction. However, in the normal direction, the system shows higher sensitivity on the optical properties for similar in size corrugations leading to reduced stable operation for higher material conductivity. Furthermore, in non-conservative systems, the Melnikov function with the Poincaré portrait analysis was combined to probe the possible occurrence of chaotic motion. During lateral actuation, systems with more conductive materials and/or the same but high corrugations exhibit lower possibility for chaotic motion. By contrast, during normal motion, chaotic behavior leading to stiction of the moving components is more likely to occur for systems with more conductive materials and similar in magnitude corrugations.

Due to widespread attention on micro/nanoelectromechanical systems (MEMS/NEMS) from the scientific and technology point of views, Casimir forces, as an omnipresent effect, become inevitably important during device actuation. Beyond the normal Casimir force, the lateral Casimir force between corrugated surfaces provides a possibility for friction-less motion without any physical contact between components, where this coupling between the two surfaces is mediated by quantum vacuum. Our findings reveal that the change of the normal Casimir force by making lateral displacement between components with corrugated surfaces will affect the dynamical actuation of devices so that the occurrence of chaotic motion could eventually lead into permanent adhesion, a phenomenon known as stiction. However, actuation under the influence of the Casimir force along the lateral direction, the larger but similar in size corrugations and/or higher material conductivity is a better choice to ensure stable operation against a chaotic motion and improve the long-term performance of devices. On the other hand, if normal motion occurs, the system reveals higher sensitivity on the optical properties for similar in size corrugations, which is amplified by increasing the value of the corrugations. In this case, chaotic behavior leading to stiction of the moving components is more likely to occur for systems with more conductive materials and similar in magnitude corrugations.

I. INTRODUCTION

Nowadays, the advancement in fabrication techniques leads to the advent of miniaturized mechanical devices such as micro/nanoelectromechanical systems (MEMS/NEMS). Moreover, the enormous possibilities for the application of these modern systems make them increasingly important in both science and technology.[1–7] By scaling down devices, due to the large enough

surface areas and small enough separation gaps, the omnipresent Casimir force plays inevitably a significant role in the actuation dynamics of devices, and its effect could be comparable to the electrostatic forces. Although Casimir force and electrostatic force are two typical forces to actuate micro- or nanodevices, there are several challenges at small length scales associated with friction and adhesion phenomena that require specific strategies to resolve them.[8–12]

The Casimir force as a quantum effect originates from the perturbation of quantum fluctuations of the electromagnetic field (EM) field,[3] as it was described in 1948 by Casimir assuming two perfectly conducting parallel plates.[5] Soon after in the 1950s, Lifshitz and co-workers[7] considered the general case of real dielectric plates by exploiting the fluctuation–dissipation theorem, which is related to the dissipative properties of matter (via optical absorption by many microscopic dipoles) and the resulting EM fluctuations. This theory describes the attractive interaction due to quantum fluctuations for all separations covering both the Casimir (long-range) and van der Waals (short-range) regimes.[1–7,13] The Casimir force is strongly dependent on the geometry and optical properties of the system,[14–24] thermal effects,[25–28] and the presence of corrugated boundaries between interacting bodies.[3,19,29,30] The latter point enables the feasibility to tailor the direction and strength of the Casimir force and consequently drive the actuation dynamic of NEMS/MEMS.

In micro/nanodevices, it is possible to produce Casimir forces both in the normal and lateral directions. The normal Casimir force is perpendicular to the surface of the interacting components, while the lateral Casimir force can be generated by moving asymmetrically the interacting bodies and its direction is tangential to the surfaces.[30,31] The lateral Casimir force between corrugated surfaces provides a possibility for friction-less motion without any physical contact between components, where this coupling between the two surfaces is mediated by quantum vacuum fluctuations. Besides all advantages of the lateral Casimir force, under certain conditions, the components of MEMS/NEMS can come into permanent adhesion, a phenomenon known as stiction. In fact, reducing the size of these devices could lead to chaotic motion that causes an abrupt change in the dynamical behavior of the system leading to stiction between actuating components.[21,22,24,32] The threshold condition for this phenomenon and its sensitivity on material optical properties are different for both the normal and lateral directions of motion.[21,29]

So far, several studies have been performed to investigate the normal Casimir force for normal displacements and the lateral Casimir force by creating tangential displacement in devices.[5–7,21,22,24] The dependence of both the normal and lateral components of the Casimir force on optical properties and thermal effects and consequently their influence on the dynamical behavior of actuating devices can be diverse.[21,29] However, there is limited knowledge on how changes of the normal Casimir force by making lateral displacement in devices with corrugated surfaces will affect the dynamical actuation of devices and the occurrence of any associated chaotic motion. Under certain conditions, the magnitude of the Casimir force can be strong enough to destroy a friction-less movement set by the lateral force leading eventually to chaotic motion and subsequently stiction. This motivated our attempt to explore here the sensitivity of the normal Casimir force on the optical properties of interacting with poor conductors, but important for future applications, during lateral movements taking also into account the corrugation amplitude of the interacting surfaces.

II. MATERIAL SYSTEMS AND DEVICE ACTUATION

Prior to modeling of the microdevice and its actuation dynamics, the starting point is the calculation of Casimir force via the Lifshitz theory (see the Appendix) with essential input of the measured imaginary part $\varepsilon''(\omega)$ of the frequency dependent dielectric function $\varepsilon(\omega)$. The optical properties of all samples here, including the system Bi_2Se_3/Al_2O_3 and the phase change material (PCM, both in crystalline and amorphous phases) AIST ($Ag_5In_5Sb_{60}Te_{30}$), were commercially characterized with ellipsometry.[16,17,23] The measurements were carried out in J.A. Woollam Co. Inc. (http://www.jawoollam.com) using the VUV-VASE (0.5–9.34 eV) and IR-VASE (0.03–0.5 eV) ellipsometers.[16,17,23] The phase change material (PCM) has an amorphous (A) semiconducting phase (with a bandgap $E_g = 0.63$ eV), and a conductive crystalline (C) phase (with a bandgap $E_g = 0.18$ eV), which yields the conductivity ratio $\omega_p^2/\omega_\tau|_{AIST(C)} 10.1$ eV.[17] PCMs are renowned for their use in optical data storage (Blue-Rays, DVDs, etc.), where they switch reversibly between the amorphous and crystalline phases without composition changes.[17] On the other hand, Bi_2Se_3 (on

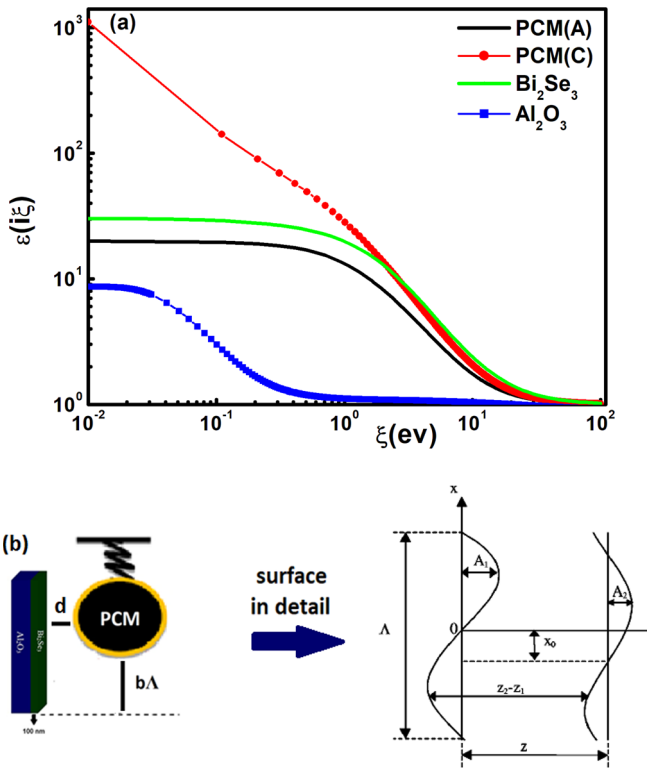

FIG. 1. (a) Dielectric functions at imaginary frequencies $\varepsilon(i\xi)$ for all materials considered in this study. (b) Concept schematic of the MEMS in this study.

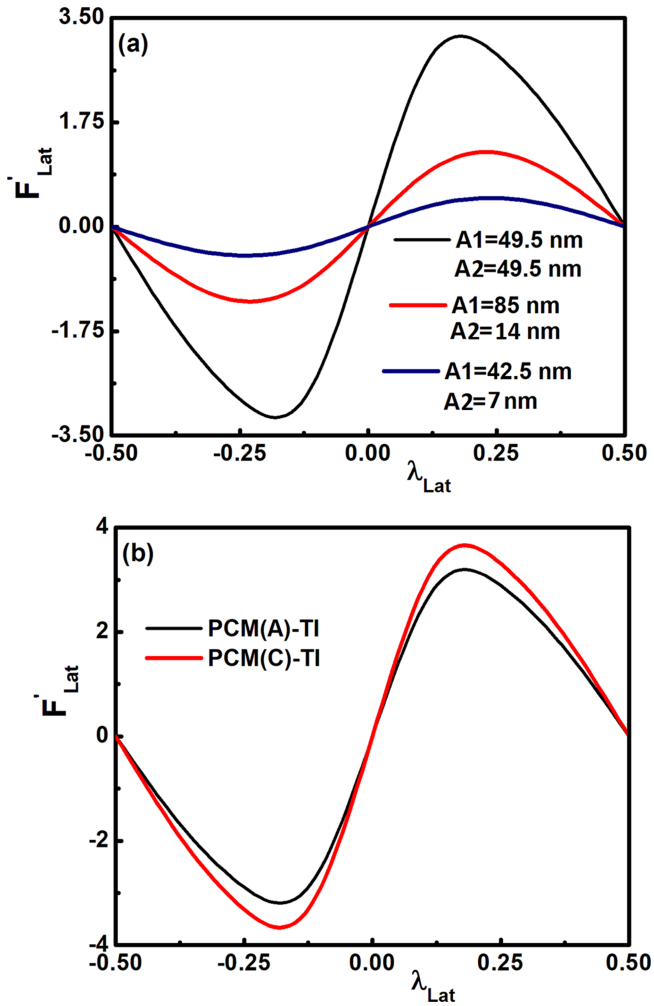

FIG. 2. (a) Lateral Casimir force vs λ_{Lat} $(= x/\Lambda)$ with different magnitude of the sinusoidal roughness. (b) Lateral Casimir force for the PCM(A)-TI and PCM(C)-TI material systems with $A_1 = A_2 = 49.5$ nm.

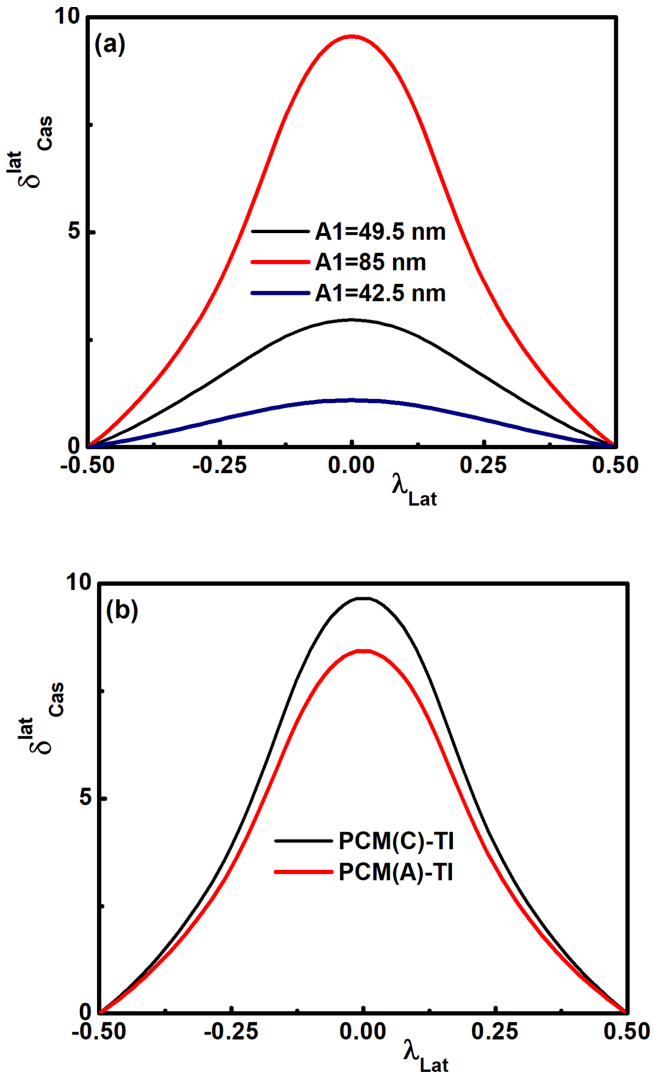

FIG. 3. Bifurcation diagram δ'^{lat}_{Cas} vs λ_{Lat} $(= x/\Lambda)$ for (a) different sets of corrugation amplitudes ($A_1 = 42.5$ and $A_2 = 7$ nm; $A_1 = 85$ and $A_2 = 14$ nm; $A_1 = 49.5$ and $A_2 = 49.5$ nm) and (b) PCM(C)-TI system with $A_1 = A_2 = 49.5$ nm.

Al_2O_3 substrates) is a well-known 3D topological insulator (TI). These materials introduce a new quantum state of matter, which are promising to make a substantial advance in future technology applications. The TIs show, in principle, an insulating gap in the bulk and gapless surface states that are protected topologically.[33–35] Figure 1(a) shows the dielectric function at imaginary frequencies $\varepsilon(i\zeta)$, which is calculated by the Kramers–Kronig relation (see the Appendix) from the measured imaginary part $\varepsilon''(\omega)$, and it is a crucial input for the subsequent calculations of the Casimir forces via the Lifshitz theory (see the Appendix). Notably, the choice of TIs and PCMs was done mainly to illustrate the involved physics of potentially interesting materials, but the results will hold also for other materials.

Furthermore, our goal is to implement the influence of the optical properties and the corrugation amplitudes on Casimir force for the sphere–plate (S–P) geometry configuration in both the lateral and normal directions, and consequently investigate the associated actuation dynamics actuation when lateral displacements take place [Fig. 1(b)]. Here, the system is composed of a fixed plate and movable sphere, where both components are assumed to be coated by TIs and PCMs, respectively, assuming operating at room temperature of 300 K. The average vertical separation in this system is considered to be $d = 200$ nm, the radius of the sphere is 100 μm, and the surface of both components is assumed to be sinusoidal corrugated.[30] In this study, we considered for comparison purposes three different sets for the corrugation amplitudes: $A_1 = 42.5$ and $A_2 = 7$ nm, $A_1 = 85$ and $A_2 = 14$ nm, and $A_1 = 49.5$ and $A_2 = 49.5$ nm for the plate and

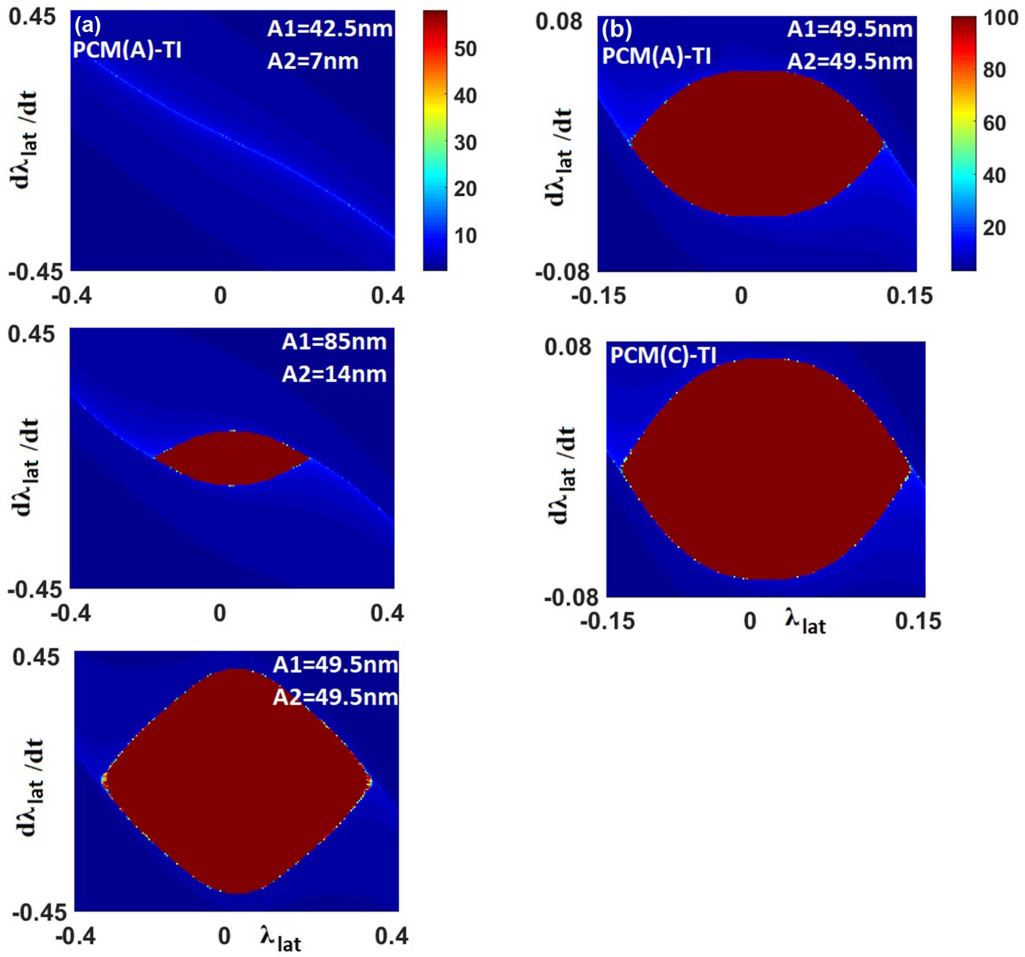

FIG. 4. Contour plot of the transient time to instability for conservative systems and initial conditions in the $\lambda_{Lat} - d\lambda_{Lat}/dT$ phase plane for (a) PCM(A)-TI, $\delta'^{lat}_{Cas} = 2$, and the magnitude of corrugations as indicated on the plots and (b) for PCM(A)-TI and PCM(C)-TI systems, $\delta'^{lat}_{Cas} = 7$ and corrugation amplitudes $A_1 = A_2 = 49.5$ nm. For the calculations, we used 150 × 150 initial conditions ($\lambda_{Lat} - d\lambda_{Lat}/dT$). The red elliptical region contains initial conditions that lead to stable oscillations. The heteroclinic orbit separates sharply stable and unstable solutions reflecting the absence of chaotic behavior.

the sphere, respectively. Also, the average period of the corrugation was assumed to be $\Lambda = 570$ nm.[30]

The equation of motion in the lateral direction is given by

$$M\frac{d^2\Delta x}{dt^2} + \varepsilon\left(\frac{M\omega_0}{Q}\right)\frac{d\Delta x}{dt} = -F^{lat}_{res} + F^{lat}_{Cas} + \gamma F_0 \cos(\omega t), \quad (1)$$

where M is the mass of the moving sphere, Δx is the lateral displacement between the components, and $(M\omega_0/Q)(d\Delta x/dt)$ is the intrinsic energy dissipation in the actuating system associated with a quality factor Q. The frequency ω_0 is assumed to be that of dynamic mode atomic force microscope (AFM) cantilevers or MEMS (typically $\omega = 300$ kHz).[30,32] The parameter γ was introduced to distinguish between the conservative (friction-less) autonomous operation of the actuating system ($\gamma = 0$) and the non-conservative driven system by an external force ($\gamma = 1$) in the presence of dissipation (friction) having a finite quality factor Q. In practice, for a conservative system, we consider MEMS with a high quality factor $Q > 10^4$, so that we can neglect any dissipation effects. In Eq. (1), the lateral Casimir force F^{lat}_{Cas} was calculated by means of the Lifshitz formula using the PFA (proximity force approximation, see the Appendix).[30] Furthermore, the lateral Casimir force is opposed by the lateral elastic restoring force $F^{lat}_{res} = -K_{lat}\,\Delta x$, where K_{lat} is the spring constant in the lateral direction.

By making lateral displacement, the normal separation between the surfaces changes leading to changes in the normal Casimir force between the interacting components. The equation of motion in the

normal direction can be written as

$$M\frac{d^2\Delta z^{rms}}{dt^2}+\varepsilon\left(\frac{M\omega_0}{Q}\right)\frac{d\Delta z^{rms}}{dt}=-F_{res}^{Nor}+F_{Cas}^{Nor}+\gamma F_0\cos(\omega t), \tag{2}$$

where F_{Cas}^{Nor} presents the normal amplitude of Casimir force, and F_{res}^{Nor} ($\approx K_{Nor}\,\Delta z^{rms}$) is the normal restoring force that resists any bending along the normal to the surfaces. Δz^{rms} describes the rms roughness amplitude as in Refs. 36 and 37,

$$\Delta z^{rms}=\sqrt{\frac{1}{\Lambda}\int_0^{\Lambda}\left(d+A_1\sin\left(\frac{2\pi x}{\Lambda}+\frac{2\pi\Delta x}{\Lambda}\right)-A_2\sin\left(\frac{2\pi x}{\Lambda}\right)\right)^2 dx}. \tag{3}$$

III. LATERAL ACTUATION DYNAMICS

(a) **Conservative system ($\gamma = 0$):** Figure 2 demonstrates the influence of the corrugation amplitude and optical properties on the lateral Casimir force during a lateral movement by one period of the sphere–plate system. Clearly, the corrugation amplitude has strong influence on the lateral Casimir force, which becomes more significant for high but similar in size amplitudes of the interacting surfaces. Moreover, the lateral force increases by increasing the conductivity of the interacting materials, as it is the case of the crystalline PCM state that has higher conductivity with respect to the amorphous state. In order to discuss the effect of the optical properties and the corrugation amplitude on the actuation of the microsystem, we introduce the bifurcation parameter $\delta_{Cas}^{lat}=F_{res}^{lat(M)}/F_{Cas}^{lat(m)}$ that represents the ratio of the maximum lateral restoring force ($F_{res}^{lat}(M)=-K_{lat}\,b\Lambda$) to the minimum lateral Casimir force. In terms of δ_{Cas}^{lat}, Eq. (1) can be written in the more convenient form as

$$\frac{d^2\lambda_{lat}}{dT^2}=-\lambda_{lat}+\frac{1}{\delta_{Cas}^{\prime lat}}\frac{F_{Cas}^{lat}}{F_{Cas}^{lat(m)}}, \tag{4}$$

where $\lambda_{lat}=\Delta x/\Lambda$, $T=\omega_0 t$, and $\delta_{Cas}^{\prime lat}=b\delta_{Cas}^{lat}$. The equilibrium points for the conservative motion can be found by setting the right part of Eq. (1) equal to zero and obtain $\delta_{Cas}^{\prime lat}=(1/\lambda_{lat})(F_{Cas}^{lat}/F_{Cas}^{lat(m)})$.

The bifurcation diagrams in Fig. 3 illustrate how the corrugation amplitude and the optical properties affect in a complex manner the stable (below the curves) regions over one period for a system due to the lateral Casimir force. The strongest effect in Fig. 3(a) corresponds to the curve with the same corrugation amplitudes, while in Fig. 3(b), the more conductive system corresponds to the upper curve indicating higher stability. The counterbalance between the lateral Casimir force and the restoring force can lead the system to perform stable motion. By increasing the lateral displacement and consequently increasing the restoring force, the system requires a stronger lateral Casimir force to preserve stable motion for larger displacements. Therefore, the loss of stability takes place faster in the system with a weaker lateral Casimir force that corresponds to materials with lower conductivity [e.g., PCM (A)-TI system] and/or systems with smaller corrugation and significant difference between the corrugation amplitudes. Besides the bifurcation diagrams, the sensitive dependence of the actuation dynamics on the corrugation amplitude and optical properties is reflected by the Poincaré portraits in Fig. 4. For the conservative system, the heteroclinic orbit separates unstable motion, where stiction occurs within one period, from the periodic closed orbits around the stable center point. As it emerges from the calculations, it is clear that the system with significant but similar corrugation and/or higher conductivity possesses larger area for the heteroclinic orbit that encloses initial conditions leading to stable operation.

(b) **Non-conservative driven lateral system ($\gamma = 1$):** The aim here is to investigate the existence of chaotic behavior of periodically driven system by an external applied force $F_o\cos(\omega t)$.[38] This phenomenon happens if the heteroclinic orbit (separatrix) splits and transversal intersections between stable and unstable orbits take place. As a starting point for the investigation, we use the Melnikov method.[37–39] If we define by $\varphi_{het}^{C}(T)$ the heteroclinic solution of the conservative system, the Melnikov function is given by[38–40]

$$M^{het}(T_0)=\frac{1}{Q}\int_{-\infty}^{+\infty}\left(\frac{d\varphi_{het}^{C}(T)}{dT}\right)^2 dT+\frac{F_0}{F_{res}^{nor\ (MAX)}}\times\int_{-\infty}^{+\infty}\frac{d\varphi_{het}^{C}(T)}{dT}\cos\left[\frac{\omega}{\omega_0}(T-T_0)\right]dT. \tag{5}$$

The splitting of the separatrix takes place if the Melnikov

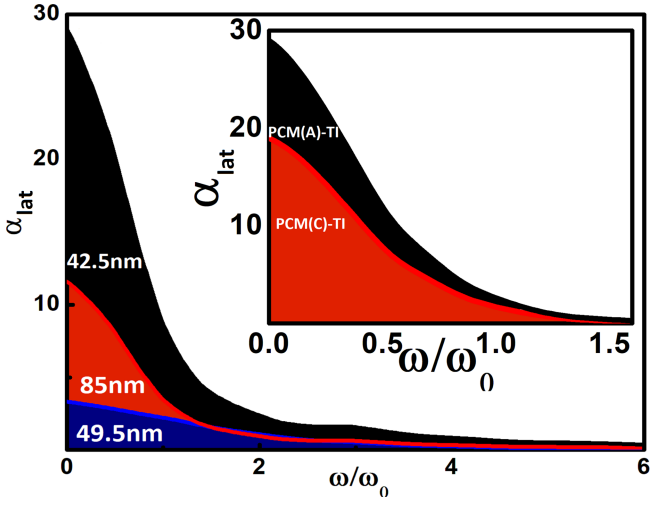

FIG. 5. Threshold curve α_{lat} ($=\gamma\omega_0 d/F_0$) vs driving frequency ω/ω_o (with ω_o being the natural frequency of the system). The area below the curve defines the condition that can possibly lead to chaotic motion. PCM(A)-TI system with different sets of corrugation amplitudes where only the A_1 is indicated ($A_1 = 42.5$ and $A_2 = 7$ nm; $A_1 = 85$ and $A_2 = 14$ nm; $A_1 = 49.5$ and $A_2 = 49.5$ nm); the values of $\delta_{Cas}^{\prime lat}$ is 0.9. Inset: PCM(A)-TI and PCM(C)-TI systems with corrugation amplitude $A_1 = A_2 = 49.5$ nm and $\delta_{Cas}^{\prime lat} = 7$.

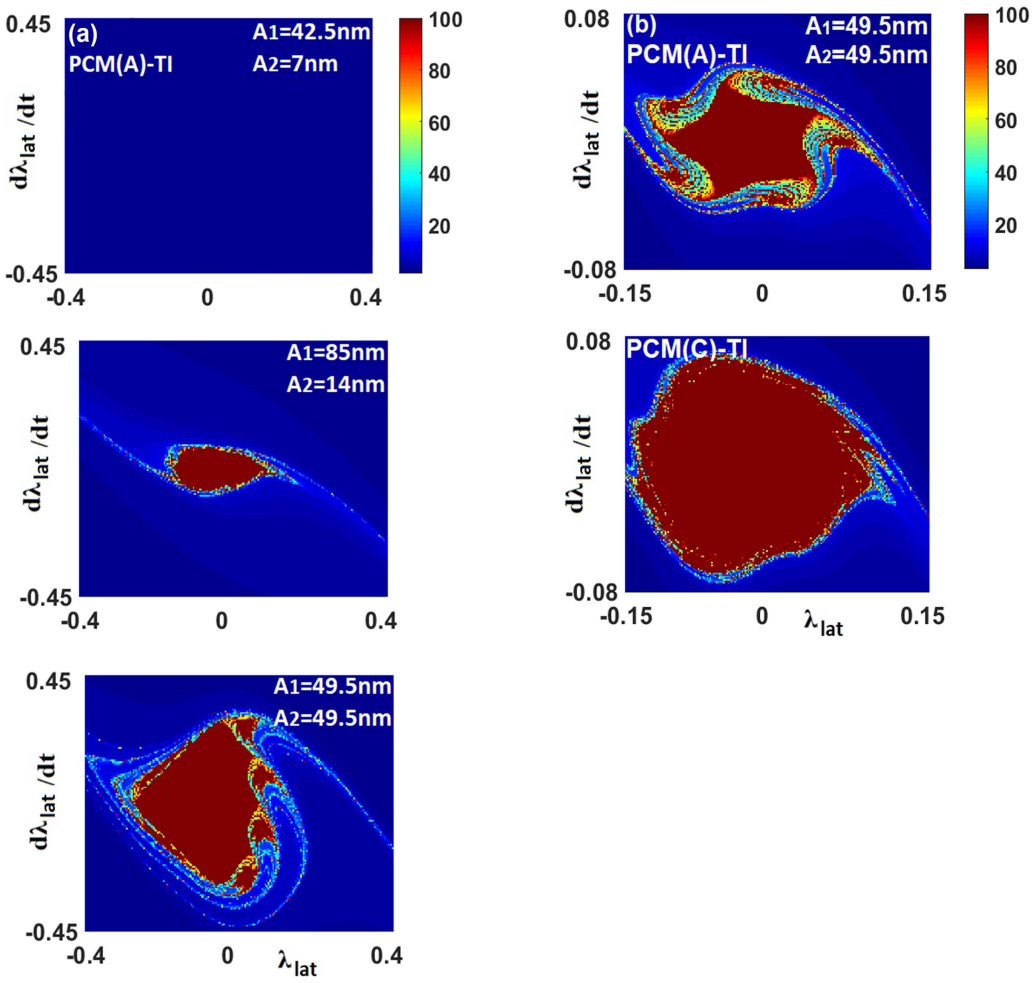

FIG. 6. Contour plot of the transient time to instability for non-conservative systems and initial conditions in the $\lambda_{Lat} - d\lambda_{Lat}/dT$ phase plane (a) PCM(A)-TI with $\alpha_{lat} = 0.5$, $\omega/\omega_o = 0.25$, and $\delta'^{lat}_{Cas} = 2$ and (b) for PCM(C)-TI and PCM(A)-TI systems with $\alpha_{lat} = 1$, $\omega/\omega_o = 0.25$, and $\delta'^{lat}_{Cas} = 7$. The materials and magnitude of corrugations are indicated. For the calculations, we used 150 × 150 initial conditions ($\lambda_{Lat} - d\lambda_{Lat}/dT$).

function has simple zeros, i.e., $M^{het}(T_0) = 0$ and $(M^{het})'(T_0) \neq 0$. The conditions of no simple zeros, where $M^{het}(T_0) = 0$ and $(M^{het})'(T_0) = 0$, provide the threshold condition for possible chaotic motion.[39,40] If we define

$$\mu^{c}_{het} = \int_{-\infty}^{+\infty} \left(\frac{d\varphi^{C}_{het}(T)}{dT} \right)^2 dT, \text{ and}$$
$$\beta_{het}(\omega) = \left| H\left[Re\left(F\left\{ \frac{d\varphi^{C}_{het}(T)}{dT} \right\} \right) \right] \right|, \quad (6)$$

with $\alpha = (1/Q)(F_0/F^{nor(MAX)}_{res})^{-1} = \Gamma\omega_0\, d/F_0, \Gamma = M\omega_o/Q$, and H[. . .] denoting the Hilbert transform, then the threshold condition for chaotic motion becomes

$$\alpha_{lat} = \beta_{het}(\omega)/\mu^{c}_{het}. \quad (7)$$

Figure 5 shows the threshold curves α_{lat} vs the driving frequency ratio ω/ω_o. The area above the curve corresponds to large values of α_{lat}, where the dissipation dominates the driving term leading to periodic motion close to the stable equilibrium point of the conservative system. However, for parameter values below the curve, the transversal intersections of stable and unstable orbits could lead to possible chaotic motion. Figure 6 shows that the area below the threshold curve becomes smaller by increasing the corrugation amplitude and becoming comparable to each other ($A_1 \approx A_2$). Moreover, according to the inset of Fig. 5, during lateral actuation, the system with reduced conductivity shows higher possibility for the occurrence of chaotic motion. Finally, Fig. 6 shows plots of the transient times to stiction for PCM(A)-TI systems with different sets

of corrugation amplitudes. Under the presence of chaotic motion, and in contrast to the conservative motion as in Fig. 4, there is a region of initial conditions where it is impossible to predict the long-term actuation state of a system. Therefore, according to Fig. 6, the system with similar but high corrugation amplitudes and materials of higher conductivity experiences stronger lateral Casimir force reducing the risk from chaotic behavior.

IV. NORMAL ACTUATION DYNAMICS

(a) **Conservative normal system ($\gamma = 0$):** Figure 7 illustrates the influence of the corrugation amplitude on the normal Casimir force for both the PCM(A)-TI and PCM(C)-TI sphere–plate systems during lateral movement. It is clear that the minimum difference in the corrugation amplitude between the moving components can provide a wider change in the normal separation during lateral movements, and this situation can be amplified by increasing the value of the corrugation. Hence, according to Fig. 7, the strongest value of the Casimir force and the widest region of change in the normal displacement belong to the system with $A_1 = A_2 = 49.5$ nm. While a medium strength of the normal Casimir force occurs for the system with $A_1 = 42.5$ and $A_2 = 7$ nm, the system that has the largest difference in corrugations ($A_1 = 85$ and $A_2 = 14$ nm) shows the smallest magnitude of the maximum normal force during lateral displacements.

In order to study the influence of the optical properties and the corrugation amplitude on the normal actuation of the microsystem,

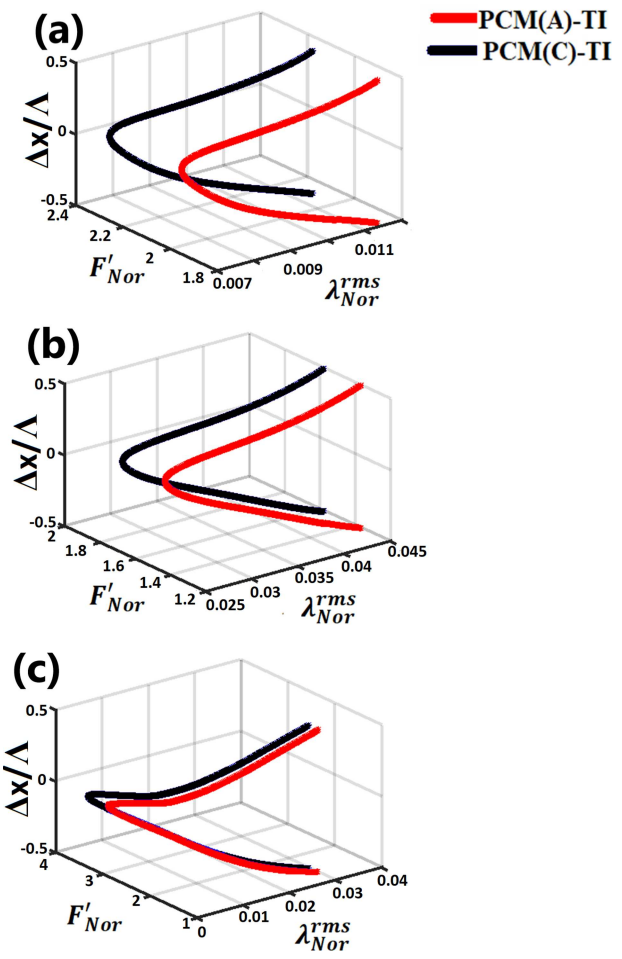

FIG. 7. Normal Casimir force vs $\lambda^{rms}_{Nor} (= \Delta z^{rms}/d)$ and vs $\Delta x/\Lambda$ (lateral displacement) for both PCM(A)-TI and PCM(C)-TI systems during one period of lateral displacement with (a) $A_1 = 42.5$ nm and $A_2 = 7$, (b) $A_1 = 85$ and $A_2 = 14$ nm, and (c) $A_1 = 49.5$ and $A_2 = 49.5$ nm.

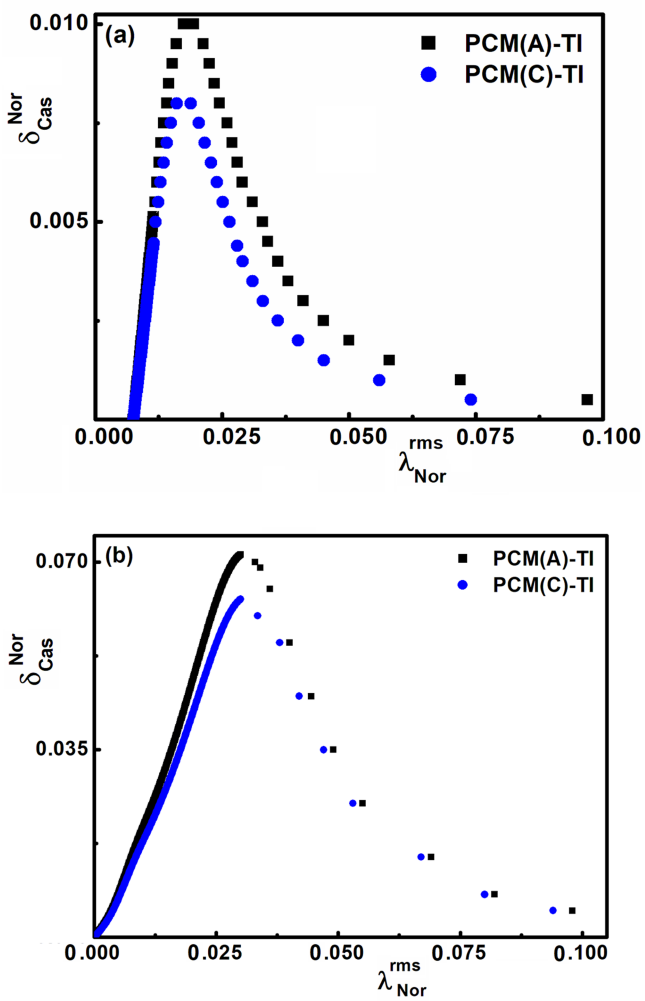

FIG. 8. Bifurcation diagrams δ^{Nor}_{Cas} vs λ^{rms}_{Nor} for different set of corrugations: (a) $A_1 = 42.5$ and $A_2 = 7$ nm; (b) $A_1 = A_2 = 49.5$ nm. All points on the left and right sides represent the stable and unstable points, respectively.

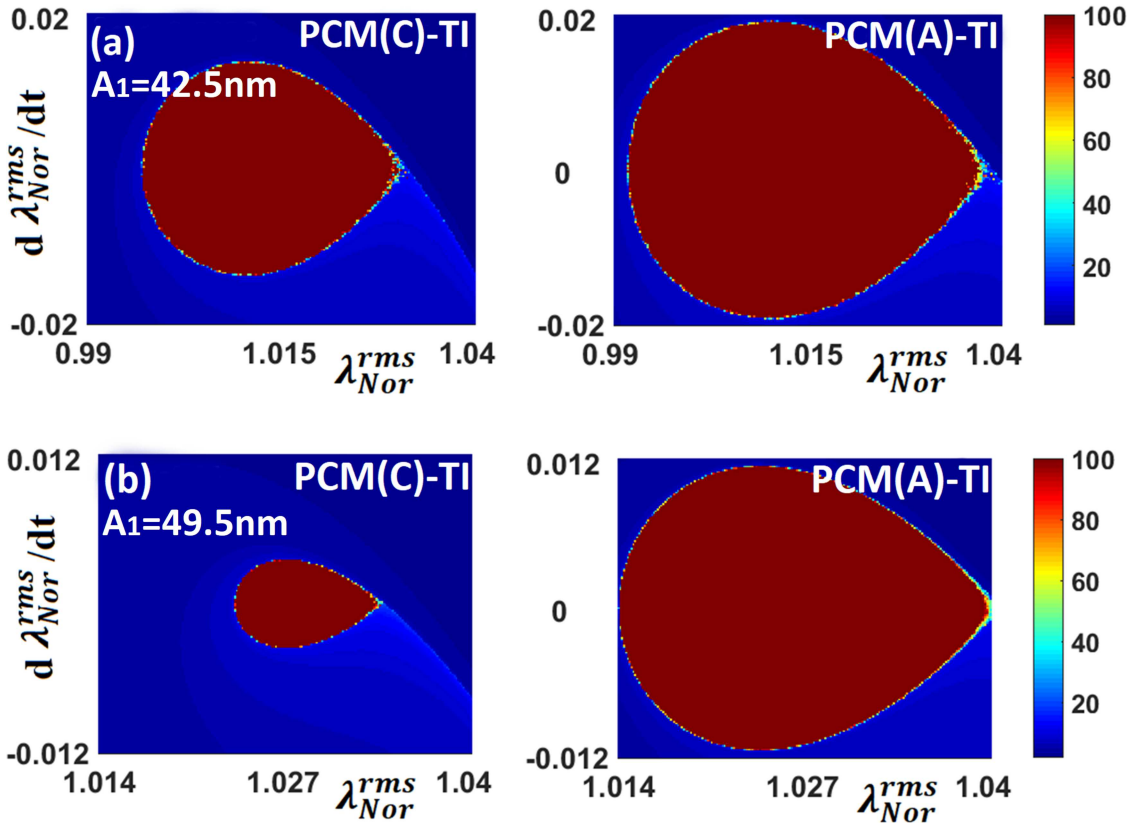

FIG. 9. Contour plot of the transient time to instability for conservative systems and initial conditions in the $\lambda_{Nor}^{rms} - d\lambda_{Nor}^{rms}/dT$ phase plane for the PCM(A)-TI and PCM(C)-TI systems. (a) The corrugations are $A_1 = 42.5$ and $A_2 = 7$ nm, and $\delta_{Cas}^{Nor} = 0.0038$. (b) The corrugations are $A_1 = 49.5$ and $A_2 = 49.5$ nm and $\delta_{Cas}^{Nor} = 0.06$. The value of δ_{Cas}^{Nor} is indicated. For the calculations, we used 150 × 150 initial conditions ($\lambda_{Nor}^{rms} - d\lambda_{Nor}^{rms}/dT$). The red elliptical region contains initial conditions that lead to stable oscillations. The homoclinic orbit separates sharply stable and unstable solutions reflecting the absence of chaotic behavior.

we introduce again the bifurcation parameter $\delta_{Cas}^{Nor} = F_{Cas}^{Nor(M)}/F_{res}^{Nor(M)}$ that represents the ratio of the maximum normal Casimir force to the maximum normal restoring force ($F_{res}^{Nor(M)} = -k_{Nor}d$). The equation of motion along the normal direction can be written in the form

$$\frac{d^2\lambda_{Nor}^{rms}}{dT^2} + \left(\frac{1}{Q}\right)\frac{d\lambda_{Nor}^{rms}}{dT} = -\lambda_{Nor}^{rms} + \delta_{Cas}^{Nor}\frac{F_{Cas}^{Nor}}{F_{Cas}^{Nor(M)}}, \quad (8)$$

with $\lambda_{Nor}^{rms} = \Delta z^{rms}/d$ and $T = \omega_0 t$. According to Fig. 8, the bifurcation analysis confirms the information obtained from Fig. 7. Due to the generation of wider normal displacement, Fig. 8(b) reveals more sensitivity to the optical properties, and the stable center points that can be created during lateral movement are separately located in the curves of both PCM(A)-TI and PCM(C)-TI systems. Figure 8(a), due the limited normal separation, reveals only a slight sensitivity to the optical properties since the stable center points in both PCM (A)-TI and PCM (C)-TI systems are located close to each other. Nevertheless, these differences lead to significant difference in the stable performance of the device as it is clearly illustrated by the Poincaré portraits in Fig. 9(a). In both systems with corrugations $A_1 = 42.5$ and $A_2 = 7$ nm, as well as $A_1 = A_2 = 49.5$ nm, the sensitivity to optical properties along the normal direction is distinct. However, as Fig. 9(b) shows, for higher value of the bifurcation parameter δ_{Cas}^{Nor}, significant shrinkage of the area enclosed by the homoclinic orbit takes place indicating higher sensitivity on the optical properties for the same level of surface corrugations.

(b) **Non-conservative normal system ($\gamma = 1$):** Similar to Sec. III, by applying the periodic external force to MEMS [$(F_o \cos(\omega t))$] and using the Melnikov method, we studied the occurrence of chaotic motion along the normal actuation. If $\varphi_{hom}^{C}(T)$ describes the homoclinic solution of the conservative system performing normal motion, the Melnikov function $M^{hom}(T_0)$ is given by

$$M^{hom}(T_0) = \frac{1}{Q}\int_{-\infty}^{+\infty}\left(\frac{d\varphi_{hom}^{C}(T)}{dT}\right)^2 dT + \frac{F_0}{F_{res}^{Nor(M)}} \times \int_{-\infty}^{+\infty}\frac{d\varphi_{hom}^{C}(T)}{dT}\cos\left[\frac{\omega}{\omega_0}(T+T_0)\right]dT. \quad (9)$$

The conditions of no simple zeros $[M^{hom}(T_0) = 0$ and $(M^{hom})'(T_0) = 0]$ provides the threshold condition for possible chaotic motion. Using these definitions, we obtain

$$\mu^{c}_{hom} = \int_{-\infty}^{+\infty} \left(\frac{d\varphi^{C}_{hom}(T)}{dT}\right)^{2} dT, \text{ and}$$
$$\beta_{hom}(\omega) = \left|H\left[Re\left(F\left\{\frac{d\varphi^{C}_{hom}(T)}{dT}\right\}\right)\right]\right|. \quad (10)$$

Similar to Eq. (7), the threshold condition for chaotic motion becomes

$$\alpha_{Nor} = \beta_{hom}(\omega)/\mu^{c}_{hom}. \quad (11)$$

Figure 10 shows the threshold curves α_{Nor} vs the driving frequency ratio ω/ω_o. It is obvious that by increasing the material conductivity, the area below the threshold curve becomes larger, which is also more prominent for corrugations of similar in size amplitude. Therefore, actuating systems with significant and similar in size amplitude of corrugations and/or with high conductivity materials can experience higher possibility toward chaotic motion leading eventually to stiction. Figure 11 further confirms this behavior, where the Poincaré portraits show that the sensitivity to the optical properties becomes more significant in a system with the same high corrugation amplitude if normal actuation takes place during lateral motion.

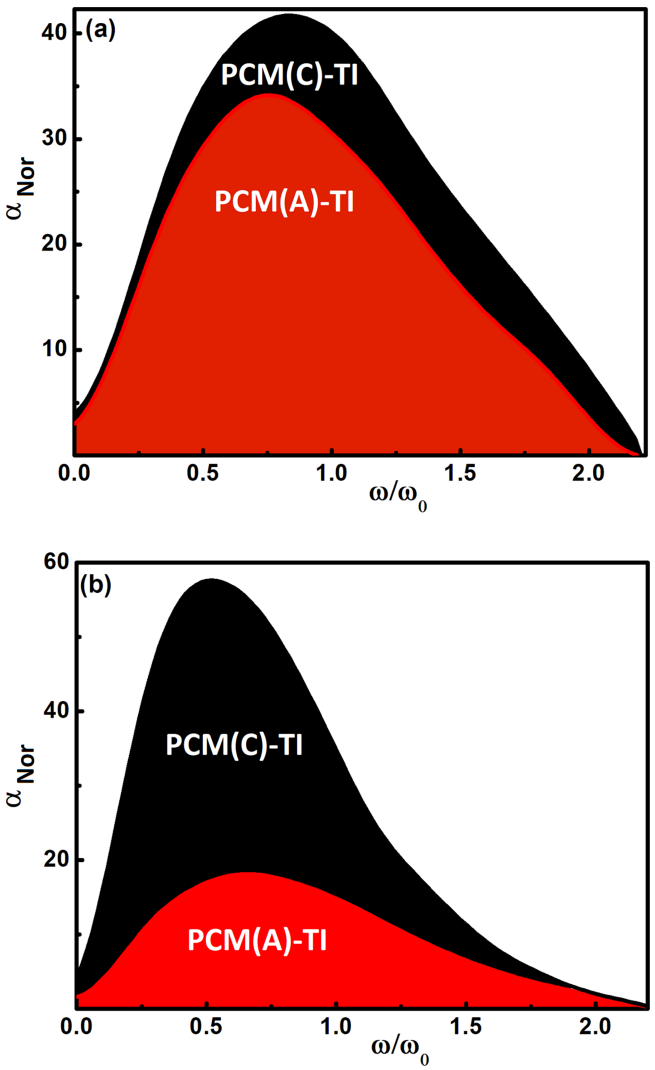

FIG. 10. Threshold curve α_{Nor} $(= \gamma\omega_0 d/F_0)$ vs driving frequency ω/ω_o (with ω_o being the natural frequency of the system). The area below the curve defines the condition that can possibly lead to chaotic motion. The values of δ^{Nor}_{Cas} and the corrugation amplitudes are (a) $\delta^{Nor}_{Cas} = 0.0038$, $A_1 = 42.5$, and $A_2 = 7$ nm; (b) $\delta^{Nor}_{Cas} = 0.061$, $A_1 = 49.5$, and $A_2 = 49.5$ nm.

V. CONCLUSIONS

In summary, we have investigated the influence of the lateral and normal Casimir force on the actuation dynamics between sinusoidal corrugated surfaces undergoing both normal and lateral displacements. The sensitivity of the actuation dynamics on the corrugation amplitudes and optical properties was explored for topological insulators and phase change materials, which are of high interest materials for device applications. The results show that the lateral Casimir force becomes stronger not only by increasing the material conductivity but also by increasing the corrugation amplitudes of both surfaces, especially toward similar in magnitude surface undulations. The latter geometry configuration produces wider normal separations during lateral motion. In a conservative system, using the bifurcation and Poincaré portrait analysis, it is shown that by increasing the corrugation amplitudes toward similar sizes and/or increasing the material conductivity, stable motion is favored along the lateral direction. However, in the normal direction, higher sensitivity on optical properties takes place for similar size corrugation amplitudes leading to reduced stable operation by increasing material conductivity. For non-conservative systems, the Melnikov function in combination with the Poincaré portrait analysis was used to probe the possible occurrence of chaotic motion. During lateral actuation, systems with more conductive materials and/or the same but high corrugation amplitudes exhibit lower possibility for the occurrence of chaotic motion. By contrast, in the normal direction, chaotic motion is more likely to occur to systems with more conductive materials and similar in magnitude corrugation amplitudes. Therefore, our results show that if during lateral actuation normal motion takes place, then the possibility of chaotic behavior toward stiction can be increased due to the normal movements. Hence, proper care must be devoted to increase the stiffness of the actuating components to prevent these additional instabilities due to cross interaction between normal and lateral displacements. Although the choice of PCMs and TIs[16,17,23] was done mainly to illustrate the involved physics of potentially interesting materials, the results will hold qualitatively also for other materials.

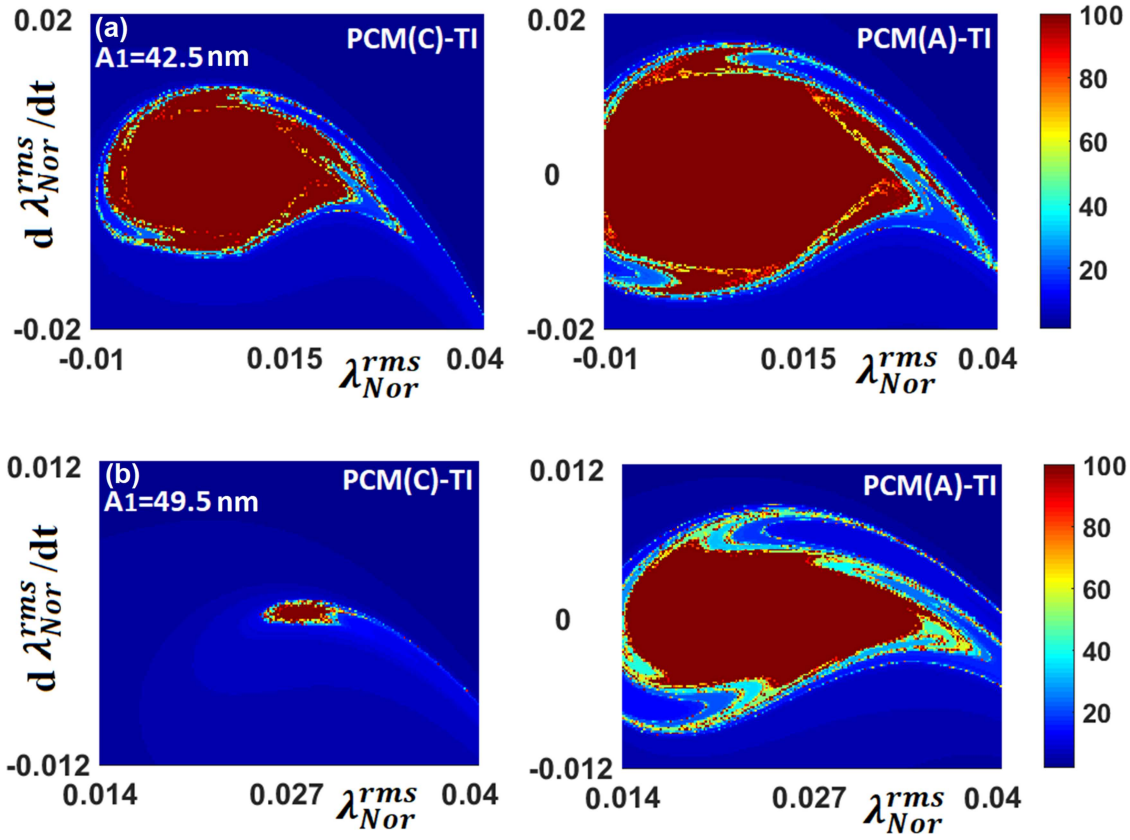

FIG. 11. Contour plot of the transient time to instability for non-conservative systems and initial conditions in the $\lambda_{Nor}^{rms} - d\lambda_{Nor}^{rms}/dT$ phase plane for PCM(A)-TI and PCM(C)-TI (a) with $\alpha_{Nor} = 1$, $\omega/\omega_o = 1$, and $\delta_{Cas}^{Nor} = 0.0038$ (the corrugations are $A_1 = 42.5$ and $A_2 = 7$ nm) and (b) with $\alpha_{Nor} = 1$, $\omega/\omega_o = 0.8$, and $\delta_{Cas}^{Nor} = 0.06$. The corrugations are $A_1 = A_2 = 49.5$ nm. For the calculations, we used 150 × 150 initial conditions ($\lambda_{Nor}^{rms} - d\lambda_{Nor}^{rms}/dT$).

ACKNOWLEDGMENTS

G.P. acknowledges support from the Netherlands Organization for Scientific Research (NWO) under Grant No. 16PR3236. F.T. acknowledges support from the Department of Physics at the Alzahra University.

APPENDIX: BRIEF THEORY OF THE CASIMIR FORCE FOR LATERAL AND NORMAL DIRECTIONS AND DIELECTRIC FUNCTION OF MATERIALS WITH EXTRAPOLATIONS

The lateral and normal Casimir forces $F_{Cas}^{lat}(z,\varphi)$ and $F_{Cas}^{nor}(z,\varphi)$, respectively, in Eqs. (1) and (2) for the plate–sphere system with sinusoidal corrugated surfaces are given (using the proximity force approximation)[30] by

$$F_{Cas}^{nor}(z,\varphi) = \nu \sum_{n=1}^{\infty} \frac{1}{n} \sum_{l=0}^{\infty\,\prime} \int_{\zeta_l}^{\infty} dyy\,[r_{TM}^{2n}(i\zeta_l, y) + r_{TE}^{2n}(i\zeta_l, y)] \times \exp(-ny)\, I_0(n\beta y), \tag{A1}$$

$$F_{Cas}^{lat}(z,\varphi) = \alpha \frac{\sin\varphi}{\beta} \sum_{n=1}^{\infty} \frac{1}{n} \sum_{l=0}^{\infty\,\prime} \int_{\zeta_l}^{\infty} dyy[r_{TM}^{2n}(i\zeta_l, y) + r_{TE}^{2n}(i\zeta_l, y)] \times \exp(-ny)\, I_1(n\beta y), \tag{A2}$$

where

$$\nu = \frac{-k_B T\ R}{4\ d^2}, \alpha = \frac{\pi k_B T\ R\ A_1 A_2}{2\ d^3 \Lambda} \text{ and } \beta = \frac{\sqrt{A_1^2 + A_2^2 - 2A_1\ A_2 \cos(\varphi)}}{z}. \tag{A3}$$

We have considered $z = d + \Delta z^{rms}$, and in addition F'_{Nor} and F'_{lat} are described by $F_{Cas}^{nor}(z,\varphi)/\nu$ and $F_{Cas}^{lat}(z,\varphi)/\alpha$, respectively; $\varphi = 2\pi\ \Delta x/\Lambda$. The prime in the first summation of Eqs. (A1) and (A2) indicate that the term corresponding to $l = 0$ should be multiplied with a factor of 1/2. Also, we have $y = 2dq_l$ with $q_l = \sqrt{k_\perp^2 + \xi_l^2/c^2}$ and ξ_l is the imaginary frequency. The Fresnel reflection coefficients are given by $r_{TE}^{(i)} = (k_0 - k_i)/(k_0 + k_i)$ and $r_{TM}^{(i)} = (\varepsilon_i\ k_0 - \varepsilon_0\ k_i)/(\varepsilon_i\ k_0 + \varepsilon_0\ k_i)$ for the transverse electric (TE)

and magnetic (TM) field polarizations, respectively. $\varsigma_l = 2\,d\,\xi_l/c$ and $k_i = \sqrt{\varepsilon_i\,(i\xi_l) + k_\perp^2}$ $(i = 0, 1, 2)$ represents the out-off plane wave vector in the gap between the interacting plates (k_0) and in each of the interacting plates ($k_{i=(1,2)}$). $k_\perp$ is the in-plane wave vector.

Furthermore, $\varepsilon(i\xi)$ is the dielectric function evaluated at imaginary frequencies, which is the essential input for calculating the Casimir force between real materials using the Lifshitz theory. Thus, $\varepsilon(i\xi)$ can be written as[11]

$$\varepsilon(i\xi) = 1 + \frac{2}{\pi}\int_0^\infty \frac{\omega\,\varepsilon''(\omega)}{\omega^2 + \xi^2}\,d\omega. \tag{A4}$$

For the calculation of the integral in Eqs. (A1) and (A2), one must use the measured data for the imaginary part $\varepsilon''(\omega)$ of the frequency dependent dielectric function $\varepsilon(\omega)$. The experimental data for the imaginary part of the dielectric function cover only a limited range of frequencies ω_1 $(= 0.03\,\text{ev}) < \omega < \omega_2$ $(= 8.9\,\text{ev})$. For the case of Bi_2Se_3 and Al_2O_3 and PCM(A), there is no extrapolation because they do not have any measurable Drude tail indicating absorption for the imaginary part at low frequencies. However, in the case of PCM(C), for the low optical frequencies ($\omega < \omega_1$), we extrapolated using the Drude model,

$$\varepsilon_L''(\omega) = \frac{\omega_p^2\,\omega_\tau}{\omega(\omega^2 + \omega_\tau^2)}, \tag{A5}$$

where ω_p is the plasma frequency and ω_τ is the relaxation frequency. Furthermore, for the high optical frequencies ($\omega > \omega_2$), we extrapolated using

$$\varepsilon_H''(\omega) = \frac{A}{\omega^3}. \tag{A6}$$

Finally, using Eqs. (A4)–(A6), the function $\varepsilon(i\xi)$ for all studied materials can be written as

$$\varepsilon(i\xi)_{PCM(C)} = 1 + \frac{2}{\pi}\int_{\omega_1}^{\omega_2} \frac{\omega\varepsilon''_{exp}(\omega)}{\omega^2 + \xi^2}\,d\omega + \Delta_L\varepsilon(i\xi) + \Delta_H\varepsilon(i\xi), \tag{A7}$$

$$\varepsilon(i\xi)_{PCM(A),Bi_2Se_3,Al_2O_3} = 1 + \frac{2}{\pi}\int_{\omega_1}^{\omega_2} \frac{\omega\varepsilon''_{exp}(\omega)}{\omega^2 + \xi^2}\,d\omega + \Delta_H\varepsilon(i\xi), \tag{A8}$$

with

$$\Delta_L\varepsilon(i\xi) = \frac{2}{\pi}\int_0^{\omega_1} \frac{\omega\varepsilon''_L(\omega)}{\omega^2 + \xi^2}\,d\omega \text{ and } \Delta_H\varepsilon(i\xi) = \frac{2}{\pi}\int_{\omega_2}^{\infty} \frac{\omega\varepsilon''_H(\omega)}{\omega^2 + \xi^2}\,d\omega. \tag{A9}$$

DATA AVAILABILITY

The data that support the findings of this study are available from the corresponding author upon reasonable request.

REFERENCES

[1] A. W. Rodriguez, F. Capasso, and S. G. Johnson, "The Casimir effect in microstructured geometries," Nat. Photonics **5**, 211 (2011).
[2] F. Capasso, J. N. Munday, D. Iannuzzi, and H. B. Chan, "Casimir forces and quantum electrodynamical torques: Physics and nanomechanics," IEEE J. Sel. Top. Quantum Electron. **13**, 400 (2007).
[3] M. Bordag, G. L. Klimchitskaya, U. Mohideen, and V. M. Mostepanenko, *Advances in the Casimir Effect* (Oxford University Press, New York, 2009).
[4] R. S. Decca, D. López, E. Fischbach, G. L. Klimchitskaya, D. E. Krause, and V. M. Mostepanenko, "Precise comparison of theory and new experiment for the Casimir force leads to stronger constraints on thermal quantum effects and long-range interactions," Ann. Phys. **318**, 37 (2005); R. S. Decca, D. López, E. Fischbach, G. L. Klimchitskaya, D. E. Krause, and V. M. Mostepanenko, "Tests of new physics from precise measurements of the Casimir pressure between two gold-coated plates," Phys. Rev. D **75**, 077101 (2007).
[5] P. Ball, "Fundamental physics: Feel the force," Nature **447**, 77 (2007).
[6] H. B. G. Casimir, "On the attraction between two perfectly conducting plates," Proc. Kon. Nederland. Akad. Wetensch. **B51**, 793 (1948).
[7] E. M. Lifshitz, "The theory of molecular attractive forces between solids," Sov. Phys. JETP **2**, 73 (1956); I. E. Dzyaloshinskii, E. M. Lifshitz, and L. P. Pitaevskii, "General theory of van der Waals forces," Sov. Phys. Usp. **4**, 153 (1961).
[8] A. Ashourvan, M. F. Miri, and R. Golestanian, "Noncontact rack and pinion powered by the lateral Casimir force," Phys. Rev. Lett. **98**, 140801 (2007).
[9] M. F. Miri and R. Golestanian, "A frustrated nanomechanical device powered by the lateral Casimir force," Appl. Phys. Lett. **92**, 113103 (2008).
[10] A. Ashourvan, M. F. Miri, and R. Golestanian, "Rectification of the lateral Casimir force in a vibrating noncontact rack and pinion," Phys. Rev. E. **75**, 040103 (2007).
[11] F. M. Serry, D. Walliserand, and G. J. Maclay, "The role of the Casimir effect in the static deflection and stiction of membrane strips in microelectromechanical systems (MEMS)," J. Appl. Phys. **84**, 2501 (1998); F. M. Serry, D. Walliser, and G. J. Maclay, "The role of the Casimir effect in the static deflection and stiction of membrane strips in microelectromechanical systems (MEMS)," J. Microelectromech. Syst. **4**, 193 (1995); G. Palasantzas and J. T. M. DeHosson, "Phase maps of microelectromechanical switches in the presence of electrostatic and Casimir forces," Phys. Rev. B **72**, 121409 (2005); G. Palasantzas and J. T. M. DeHosson, "Pull-in characteristics of electromechanical switches in the presence of Casimir forces: Influence of self-affine surface roughness," Phys. Rev. B **72**, 115426 (2005).
[12] F. W. DelRio, M. P. de Boer, J. A. Knapp, E. D. Reedy, Jr., P. J. Clews, and M. L. Dunn, "The role of van der Waals forces in adhesion of micromachined surfaces," Nat. Mater. **4**, 629 (2005).
[13] H. G. Craighead, "Nanoelectromechanical systems," Science **290**, 1532 (2000).
[14] F. Chen, G. L. Klimchitskaya, V. M. Mostepanenko, and U. Mohideen, "Demonstration of optically modulated dispersion forces," Opt. Express **15**, 4823 (2007); G. Torricelli, I. Pirozhenko, S. Thornton, A. Lambrecht, and C. Binns, "Casimir force between a metal and a semimetal," Europhys. Lett. **93**, 51001 (2011).
[15] S. de Man, K. Heeck, R. J. Wijngaarden, and D. Iannuzzi, "Halving the Casimir force with conductive oxides," Phys. Rev. Lett. **103**, 040402 (2009).
[16] G. Torricelli, P. J. van Zwol, O. Shpak, C. Binns, G. Palasantzas, B. J. Kooi, V. B. Svetovoy, and M. Wuttig, "Switching Casimir forces with phase-change materials," Phys. Rev. A **82**, 010101 (2010).
[17] G. Torricelli, P. J. van Zwol, O. Shpak, G. Palasantzas, V. B. Svetovoy, C. Binns, B. J. Kooi, P. Jost, and M. Wuttig, "Casimir force contrast between amorphous and crystalline phases of AIST," Adv. Funct. Mater. **22**, 3729 (2012).
[18] C.-C. Chang, A. A. Banishev, G. L. Klimchitskaya, V. M. Mostepanenko, and U. Mohideen, "Reduction of the Casimir force from indium tin oxide film by UV treatment," Phys. Rev. Lett. **107**, 090403 (2011).
[19] V. B. Svetovoy, P. J. van Zwol, G. Palasantzas, and J. T. M. DeHosson, "Optical properties of gold films and the Casimir force," Phys. Rev. B. **77**, 035439 (2008); G. Bimonte, "Making precise predictions of the Casimir force between metallic plates via a weighted Kramers-Kronig transform," Phys. Rev. A **83**, 042109 (2011).
[20] A. Canaguier-Durand, P. A. Maia Neto, A. Lambrecht, and S. Reynaud, "Thermal Casimir effect for Drude metals in the plane-sphere geometry," Phys. Rev. A **82**, 012511 (2010).
[21] F. Tajik, M. Sedighi, M. Khorrami, A. A. Masoudi, and G. Palasantzas, "Chaotic behavior in Casimir oscillators: A case study for phase-change materials," Phys. Rev. E **96**, 042215 (2017); F. Tajik, M. Sedighi, and G. Palasantzas, "Sensitivity on materials optical properties of single beam torsional Casimir actuation," J. Appl. Phys. **121**, 174302 (2017).
[22] F. Tajik, M. Sedighi, M. Khorrami, A. A. Masoudi, H. Waalkens, and G. Palasantzas, "Dependence of chaotic behavior on optical properties and electrostatic effects in double-beam torsional Casimir actuation," Phys. Rev. E **98**, 022210 (2018); F. Tajik, M. Sedighi, A. A. Masoudi, H. Waalkense, and G. Palasantzas,

"Sensitivity of chaotic behavior to low optical frequencies of a double beam torsional actuator," Phys. Rev. E **100**, 012201 (2019).
[23]Z. Babamahdi, V. B. Svetovoy, D. T. Yimam, B. J. Kooi, T. Banerjee, J. Moon, S. O. Enache, M. Stöhr, and G. Palasantzas, "Casimir and electrostatic forces from Bi_2Se_3 thin films of varying thickness," Phys. Rev. B **103**, L161102 (2021).
[24]F. Tajik, Z. Babamahdi, M. Sedighi, and G. Palasantzas, "Nonlinear actuation of Casimir oscillators towards chaos: Comparison of topological insulators and metals," Universe **7**, 123 (2021).
[25]M. Antezza, L. P. Pitaevskii, S. Stringari, and V. B. Svetovoy, "Casimir-Lifshitz force out of thermal equilibrium," Phys. Rev. A **77**, 022901 (2008).
[26]J. M. Obrecht, R. J. Wild, M. Antezza, L. P. Pitaevskii, S. Stringari, and E. A. Cornell, "Measurement of the temperature dependence of the Casimir-Polder force," Phys. Rev. Lett. **98**, 063201 (2007).
[27]M. Antezza, L. P. Pitaevskii, and S. Stringari, "New asymptotic behavior of the surface-atom force out of thermal equilibrium," Phys. Rev. Lett. **95**, 113202 (2005).
[28]F. Tajik, M. Sedighi, Z. Babamahdi, A. A. Masoudi, H. Waalkense, and G. Palasantzas, "Dependence of non-equilibrium Casimir forces on material optical properties towards chaotic motion during device actuation," Chaos **29**, 093126 (2019); F. Tajik, M. Sedighi, Z. Babamahdi, A. A. Masoudi, H. Waalkense, and G. Palasantzas, "Sensitivity of non-equilibrium Casimir forces on low frequency optical properties towards chaotic motion of microsystems," Chaos **30**, 023108 (2020).
[29]F. Tajik, A. A. Masoudi, M. Sedighi, and G. Palasantzas, "Chaotic motion due to lateral Casimir forces during nonlinear actuation dynamics," Chaos **30**, 073101 (2020); V. B. Svetovoy and G. Palasantzas, "Influence of surface roughness on dispersion forces," Adv. Colloid Interface Sci. **216**, 1 (2015).
[30]H. C. Chiu, G. L. Klimchitskaya, V. N. Marachevsky, V. M. Mostepanenko, and U. Mohideen, "Lateral Casimir force between sinusoidally corrugated surfaces: Asymmetric profiles, deviations from the proximity force approximation, and comparison with exact theory," Phys. Rev. B **81**, 115417 (2010); F. Chen, U. Mohideen, G. L. Klimchitskaya, and V. M. Mostepanenko, "Experimental and theoretical investigation of the lateral Casimir force between corrugated surfaces," Phys. Rev. A **66**, 032113 (2002).
[31]R. Golestanian and M. Kardar, "Mechanical response of vacuum," Phys. Rev. Lett. **78**, 3421 (1997); R. Golestanian and M. Kardar, "Path-integral approach to the dynamic Casimir effect with fluctuating boundaries," Phys. Rev. A. **58**, 1713 (1998); T. Eming, A. Hanke, R. Golestanian, and M. Kardar, "Probing the strong boundary shape dependence of the Casimir force," Phys. Rev. Lett. **87**, 260402 (2001).
[32]W. Broer, H. Waalkens, V. B. Svetovoy, J. Knoester, and G. Palasantzas, "Nonlinear actuation dynamics of driven Casimir oscillators with rough surfaces," Phys. Rev. Appl. **4**, 054016 (2015).
[33]M. Z. Hasan and C. L. Kane, "Topological insulators," Rev. Mod. Phys. **82**, 3045 (2010).
[34]J. E. Moore, "The birth of topological insulators," Nature **464**, 194 (2010).
[35]D. Hsieh, D. Qian, L. Wray, Y. Xia, Y. Hor, R. J. Cava, and M. Hasan, "Topological Dirac insulator in a quantum spin Hall phase," Nature **452**, 970 (2008).
[36]E. Gadelmawla, M. Koura, T. Maksoud, I. Elewa, and H. Soliman, "Roughness parameters," J. Mater. Process. Technol. **123**, 133 (2002).
[37]P. M. Santos and E. N. A. Júlio, "State-of-the-art review on roughness quantification methods for concrete surfaces," Constr. Build. Mater. **38**, 912 (2013).
[38]O. Degani and Y. Nemirovsky, "Design considerations of rectangular electrostatic torsion actuators based on new analytical pull-in expressions," J. Microelectromech. Syst. **11**, 20 (2002).
[39]M. Siewe and U. H. Hegazy, "Homoclinic bifurcation and chaos control in MEMS resonators," Appl. Math. Model. **35**, 5533 (2011).
[40]M. W. Hirsch, S. Smale, and R. L. Devaney, *Differential Equations, Dynamical Systems, and an Introduction to Chaos* (Elsevier Academic Press, San Diego, CA, 2004).